Int J Adv Manuf Technol (2016) 85:2597–2605
DOI 10.1007/s00170-015-8140-9

ORIGINAL ARTICLE

Microstructures and high-temperature wear performances of cathodic arc ion plating on YT14 cutting tool

Kong Dejun[1,2] · **Guo Haoyuan**[1]

Received: 17 September 2015 / Accepted: 12 November 2015 / Published online: 20 November 2015

Abstract A layer of titanium carbon nitride (TiCN) coating was deposited on YT14 cutting tool by a cathodic arc ion plating (CAIP); the friction-wear behaviors of TiCN coating at the temperatures of 200, 300, and 400 °C were investigated by a high-temperature friction-wear tester. The results show that a metallurgical bonding is formed at the TiCN coating interface, of which the bonding strength is 58.15 N measured by scratch test. The average coefficient of friction (COF) of TiCN coating at the temperatures of 200, 300, and 400 °C is 0.2931, 0.5252, and 0.4114, respectively; the wear rates increase gradually with the wear temperatures. The TiO_2 that is produced during the wear improves the lubrication of the coating; the wear mechanisms are primarily composed of oxidation wear, abrasive wear, and adhesive wear, accompanied by slight fatigue wear.

Keywords TiCN coating · Cathodic arc ion plating (CAIP) · High-temperature wear · Plane scan analysis · Line scan · Analysis

1 Introduction

With the development of high speed, high precision, dry cutting, etc., surface coating technology is a main way of improving effectively cutting tool performance [1], which significantly increases the efficiency of a wide range of manufacturing operations with intermittent and heavy cutting [2]. Titanium nitride (TiN) and titanium carbide (TiC) coatings with high hardness, high wear resistance, and chemical stability are widely used on the machine manufacturing [3, 4]; compared with the TiN and TiC coatings, titanium carbon nitride (TiCN) coating with the excellences of TiC and TiN coatings possessing lower coefficient of friction (COF) and higher wear resistance has already been known for some decades and was introduced to the market in the mid-1980s [5–8]. The TiCN coating is a solid solution of TiN and TiC with the advantages such as superior chemical stability, high wear resistance, strong oxidation resistance, and low COF, which make them a good candidate for cutting tool materials [9]. However, metal cutting is a complex process that involved with the interaction of tools and machined surfaces [10]; the TiCN coating has a lower COF than an uncoated one under similar cutting conditions, exhibiting good cutting performance and economies. The TiCN coating has a great significance of further improving the production efficiency and extending service life of the cutting tools [11–14]; researches have investigated the applications of TiCN coating at China and abroad, but little has been reported about the friction and wear mechanism of TiCN coating, especially the wear characteristics at different high temperatures. A TiCN coating was deposited on YT14 cutting tool by cathode arc ion plating (CAIP); the surface-interface morphologies, distributions of chemical elements, and phases of the TiCN coating were analyzed with a SEM, energy dispersive spectrometer (EDS), and X-ray diffractometer (XRD), respectively, and bonding strength of the TiCN coating was quantitatively characterized with a scratch test. The friction-wear behaviors of the coating at the temperatures of 200, 300, and 400 °C were investigated with a high-temperature friction-wear tester, which provided an experimental basis for the investigation of the friction behaviors

✉ Kong Dejun
kong-dejun@163.com

[1] College of Mechanical Engineering, Changzhou University, Changzhou 213164, China

[2] Jiangsu Key Laboratory of Materials Surface Science and Technology, Changzhou University, Changzhou 213164, China

and wear mechanism of TiCN coating on the YT14 cutting tools at high temperatures.

2 Experiment

The substrate material was a YT14 cutting tool with the chemical compositions as follows (mass, %): tungsten carbide (WC) 78, TiC 14, and Co 8. The samples were polished with #80–#2000 sandpapers in turn and polished to mirror with diamond grinding paste. Before being put into the vacuum chamber, the samples were cleaned with pure acetone on an ultrasonic oscillation for 10 min and dried for the deposition in a PVT coating system. To deposit TiCN coating, the industrial high-purity CH_4 and N_2 were used as the working gases and the Ti with the purity of 99.99 % was used as a target. The deposition parameters were shown as follows: vacuum of 3×10^{-3} Pa, deposition temperature of 500 °C, and deposition time of 60 min. After annealing at 180 °C for 2 h, the coating samples were cleaned with acetone on a KQ2200DE-type CNC ultrasonic cleaner, then cleaned with ultrasonic deionized water, and dried with a hair dryer; the required samples were obtained. The high-temperature friction and wear properties of TiCN coating were analyzed on a HT-1000-type high-temperature friction-wear tester. The friction mode was sliding friction, and the grinding material was a ceramic ball (Si_3N_4) with the diameter of 5 mm. The test parameters were shown as follows: wear temperatures of 200, 300, and 400 °C, respectively; speed of 500 rpm; rotation radius of 5 mm; and load of 5 N. The test temperatures and COFs were measured by computer; at the same time, the real-time graphics was displayed and the related data were stored. Bonding strength of the coating was measured quantitatively on a WS-2005-type film adhesion automatic scratch tester; the measurement method was acoustic emission, and the scratch parameters were load of 100 N, loading speed of 50 N/min, and scratch length of 6 mm. The morphologies and plane scans of the TiCN coating after high-temperature wear were observed with a JSUPRA55-type field emission scanning electron microscopy (FESEM) and its configured EDS, respectively, and the phases of the coating were analyzed with a D/max2500PC-type XRD.

3 Result analysis and discussion

3.1 Surface morphologies and EDS analysis

The coating surface appeared as a few continuous and uniform blue grays with a certain roughness; there were a few black holes and white light particles, which grew with island pattern, as shown in Fig. 1a. There was a light-shade interface between the TiCN coating and substrate. The coating thickness was about 1.75 μm, as shown in Fig. 1b; the transition layer was smooth at the bonding interface; and the coating and substrate were closely integrated to form a metallurgical bonding, which improved bonding strength of the coating. The coating appeared as fine compact structures without cracking; the columnar crystal morphology was not obvious. The EDS analysis result of the TiCN coating was shown in Fig. 1c; the coating was mainly composed of Ti, C, N, and O atoms with the mass fractions (mass, %) as follows: Ti 57.61, C 17.44, N 21.78, and O 2.15, and the atom fractions (at, %) were Ti 27.1, C 34.75, N 35.12, and O 3.03. There were a small number of O atoms; this was because the O atoms were absorbed on the coating surface when exposed in the air.

3.2 XRD analysis

Figure 2a shows the XRD analysis result of the YT14 substrate and TiCN coating at normal temperature. The diffraction peaks of WC, TiC, and Co had been detected in the substrate, which were the compositions of YT14 cutting tool sintered by the hard phases of WC, TiC, and the binder of Co. The diffraction peaks of TiCN, TiN, TiC, and TiO_2 were detected in the coating, which was mainly composed of Ti, N, and C, containing a small number of O atoms, which was consistent with the EDS analysis result in Fig. 1c. The C existed in the forms of TiC and polluted C; the N existed in the forms of TiN and TiCN; and the Ti existed in the forms of TiN, TiC, and TiO_2. The forming of TiCN was that the N position of TiN was partly replaced by C atoms to form a substitutional solid solution structure with face-centered cubic (FCC) of δ-NaCl, and the C atoms entered into the TiN lattices at a solid solution way, producing an elastic strain field. The C atoms were the center of the elastic strain field; when the dislocation movement appeared near the C atoms, the larger resistance force was produced, improving microhardness of the TiCN coating [15, 16]. Since the lattice constant of TiN was slightly smaller than that of TiC coating, the lattice constant of the TiCN coating was between TiN and TiC coatings. The TiCN coating had a strong preferential growth along the direction of crystal face (111); this was because the crystal face (111) was the dense face and the TiCN coating was preferentially grown at the direction of crystal face (111), which had a significant effect on the enhancing of the coating microhardness. Figure 2b shows the XRD analysis results of the coatings at different temperatures. There were TiCN, TiC, TiN, and TiO_2 phases at the temperatures of 200, 300, and 400 °C, without new phases, indicating that the phases only changed in the quantity and no new substances were produced during the wear. The diffraction peak of TiCN phase in the coating was still very strong, which indicated that the coating had not been completely oxidized at 400 °C and still had the ability of resisting high-temperature oxidation.

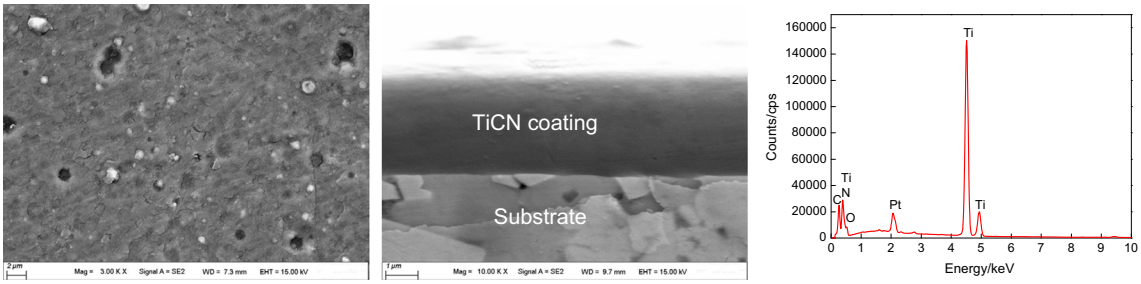

(a) Surface morphology (b) Interface morphology (c) EDS analysis

Fig. 1 Surface-interface morphologies and EDS analysis of TiCN coating. **a** Surface morphology. **b** Interface morphology. **c** EDS analysis

3.3 Bonding strength

The bonding strength of the TiCN coating was assessed with an automatic scratch method, the load of the coating spalling was determined with emission signals, and the interfacial bonding strength was characterized with the critical load. Figure 3a shows the scratch morphology of TiCN coating. The TiCN coating had a good binding ability with the bonding strength of 58.15 N, as shown in Fig. 3b. This was because ion bombardment with high energy activated the atoms on the substrate surface, and the diffusion and displacement produced a metallurgical bonding at the interface, improving the coating density.

3.4 COFs and wear rate

Figure 4a shows the relationship between the COFs of the coating and wear time under the load of 5 N at the temperatures of 200, 300, and 400 °C. The friction process of TiCN coating was divided into running-in period and stable stage; the COFs did not fluctuate at the wear end, which indicated that the coating did not fail after wear. In the running-in period, the COF of the TiCN coating was presented bigger, due to its surface roughness. When the temperatures increased, the coating hardness reduced, resulting in increasing of the COFs. As the wear time increased to 5 min, the TiO_2 compounds were produced to act as a lubricant in sliding wear situations [17]; the COF decreased and was stable in stable stage. The COF of the TiCN coating was the lowest at 200 °C, and the average COF of the coating was 0.2931 within 30 min. The running-in period was short, and the COF rapidly increased; the average value was 0.7123, because the microconvex body on the coating surface made the friction force sharply increase at the contact initial stage of friction pair. The average COF was 0.2838 at the stable stage, decreasing by 60.16 %, compared with that at the running-in period; this was because the transition layer of amorphous C had a role of reducing COFs on the friction surface. The average COF of the coating was 0.5252 within 30 min at 300 °C, increasing by 79.19 % compared with that at 200 °C. In addition, the average COF of the coating increased sharply to 0.5711 in the running-in period, decreasing by 19.82 % compared with that at 200 °C, while that of the coating in the stable stage was 0.4851, increasing by 70.93 %; this was because the hardness of the coating decreased with the temperature increasing and the COF of the TiCN coating increased under dry friction condition. The average COF of the TiCN coating within 30 min was 0.4114; compared with those at 200 and 300 °C, the COF of the coating increased by 40.36 % and decreased by 21.67 %, respectively. The average COF of the TiCN coating was 0.4305

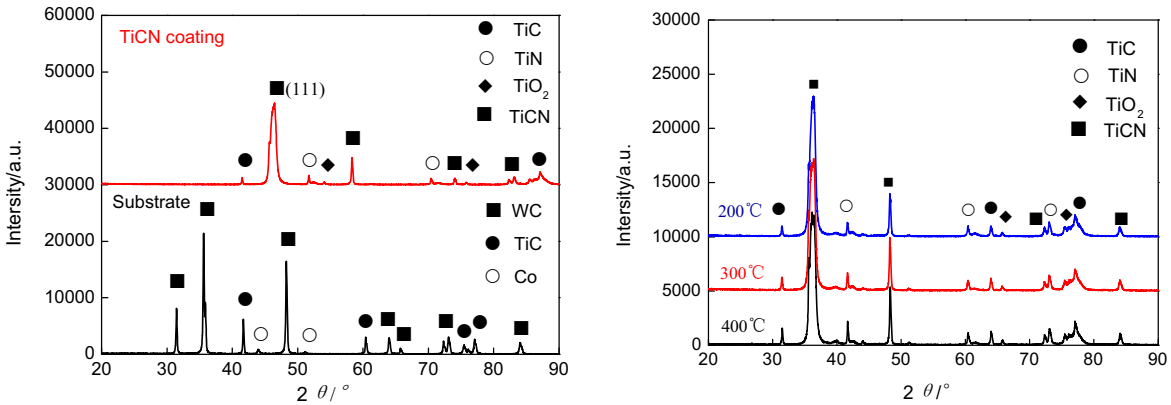

(a) Phases of TiCN coating and substrate at normal temperature (b) Phases of TiCN coating at different high temperatures

Fig. 2 XRD analysis of TiCN coating and substrate. **a** Phases of TiCN coating and substrate at normal temperature. **b** Phases of TiCN coating at different high temperatures

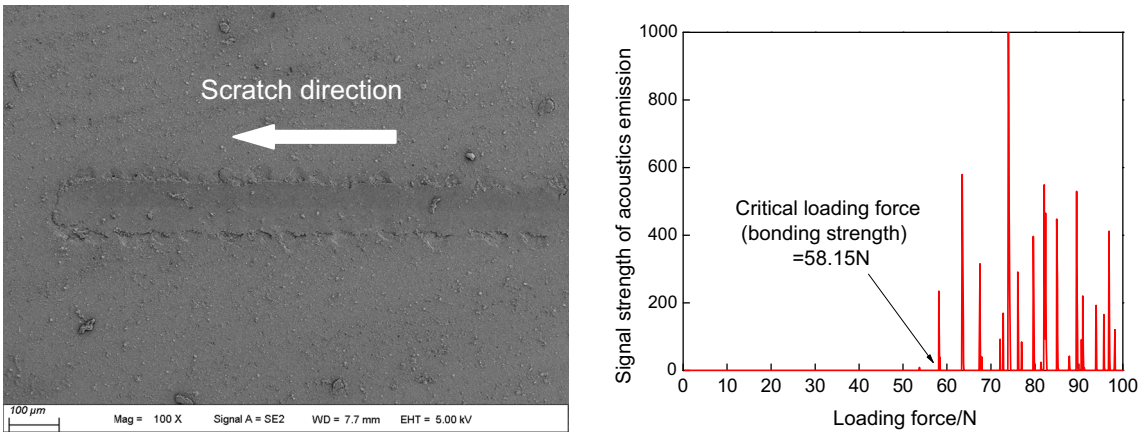

(a) Scratch morphology (b) Interfacial bonding strength

Fig. 3 Scratch morphology and bonding strength of TiCN coating. **a** Scratch morphology. **b** Interfacial bonding strength

in the running-in period at 400 °C, compared with that at 300 °C, the COF decreasing by 24.62 %. The fluctuation of COF in the running-in period was larger; this was because the TiCN coating existed roughness, the contact area of the microconvex body was small, and the contact stress was big, which resulted in the friction resistance increasing. After the particle surface being worn, the actual contact area increased gradually. The coating was gradually oxidized to form an oxide film of TiO_2 during the friction at high temperatures, which played a role of lubrication and antifriction; therefore, the COFs decreased slowly and tended to be gentle. The average COF of the coating was 0.3998 at the stable stage, and the fluctuation of the COFs was small, which indicated that the coating had a good lubricating effect, improving abrasive wear and adhesive abrasion resistance. Figure 4b shows the relationship between wear rates and high temperatures. The wear rate of the coating at 200, 300, and 400 °C was 0.005, 0.011, and 0.019 nm^3/N, respectively, indicating that the wear rates of the TiCN coating increased with the temperatures; this is because the TiCN coating was softened and oxidized, and the grinding ball produced macrocutting friction on the oxidized coating and formed the furrow surface, which increased the wear rates of the coatings. From the above analyses, the COFs of the TiCN coating increased with the temperature increasing and the wear rates also increased with the temperature at the range of 200–400 °C.

3.5 Plane scan analysis of worn scar

3.5.1 Plane scan analysis of worn scar at 200 °C

Figure 5a shows the plane scanned position of worn scar at 200 °C. The wear on the coating surface was slight, and the wear rate was smaller. There was a small amount of debris accumulated on both sides of worn scar, which came from the two aspects: (1) the discharge of debris was aggregated on both sides of worn scar and (2) the coating surface produced plastic flowing during the reciprocating wear under high pressure. Figure 5b shows the EDS analysis result of the worn scar with the mass fractions (mass,%) as follows: Ti 54.54, C

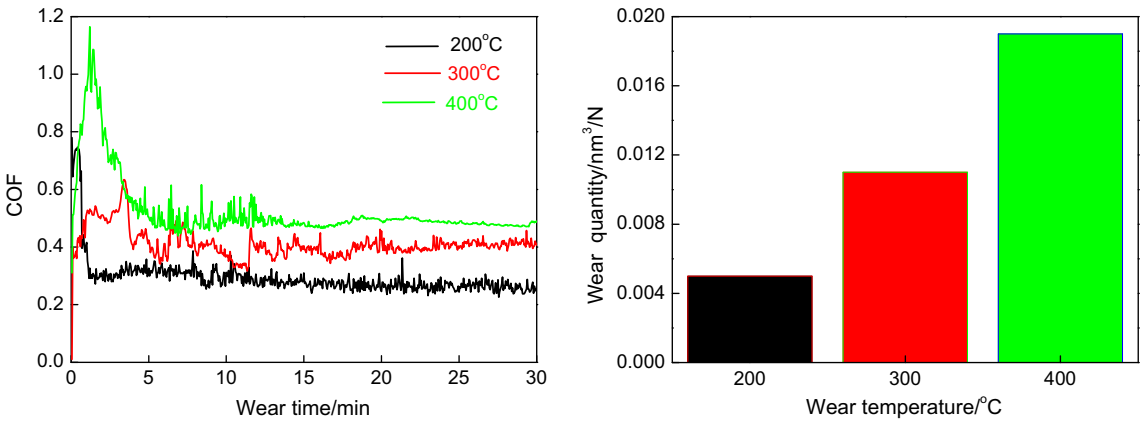

(a) COFs vs wear time (b) Wear rates vs temperatures

Fig. 4 COFs and wear rate. **a** COFs versus wear time. **b** Wear rates versus temperatures

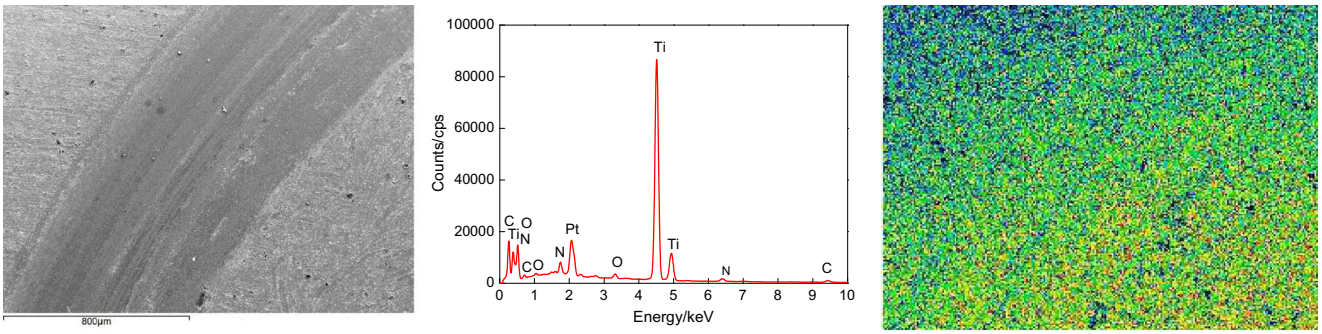

(a) Scanned position (b) Result of plane scan (c) Ti content

(d) C content (e) N content

(f) O content (g) Si content

Fig. 5 Plane scans of worn scar on TiCN coating at 200 °C. **a** Scanned position. **b** Result of plane scan. **c** Ti content. **d** C content. **e** N content. **f** O content. **g** Si content

15.78, N 19.16, O 10.26, and Si 0.26, and the atom fractions (at, %)were as follows: Ti 25.42, C 29.41, N 30.16, O 14.35, and Si 0.21. The contents of Ti, C, and N atoms of the worn scar had declined compared with those of original sample. The plane scans of Ti, C, and N elements in Fig. 5c–e were dim, which indicated that the atom fractions decreased on the worn scar. The content of O atom on the worn scar increased from 3.03 to 14.35 %, which was brighter, showing that the content of O atoms increased. The TiCN coating was slightly oxidized during the wear, as shown in Fig. 5f. A small number of Si atoms were also detected on the worn scar, which indicated that the surface of the grinding ball was stunk on the worn scar and gathered on the worn scar with the form of worn debris, as shown in Fig. 5g. The W and Co atoms were not detected, indicating that the TiCN coating was not worn out at 200 °C.

3.5.2 Analysis of wear scar surface at 300 °C

Figure 6a shows the plane scanned position of worn scar at 300 °C. The cutting effect of grinding ball was obvious, the worn scar of the TiCN coating was wider, and the wear was more serious than that at 200 °C, which belonged to abrasive wear. Figure 6b shows the EDS analysis result of the worn scar with the mass fractions (mass, %) as follows: Ti 55.94, C 14.37, N 15.24, O 14.17, and Si 0.28; and the atom fractions (at, %) were as follows: Ti 26.81, C 27.55, N 25.04, O 20.37, and Si 0.23. The contents of N, C, and Ti decreased compared

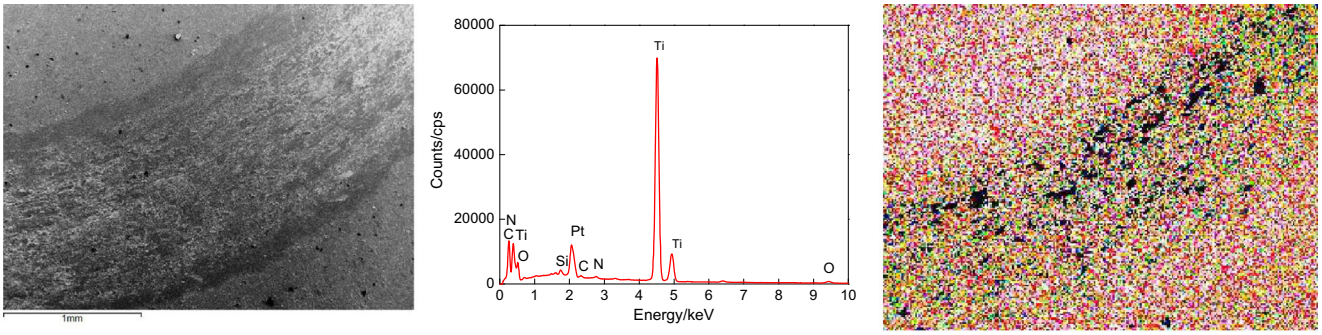

(a) Scanned position (b) Result of plane scan (c) Ti content

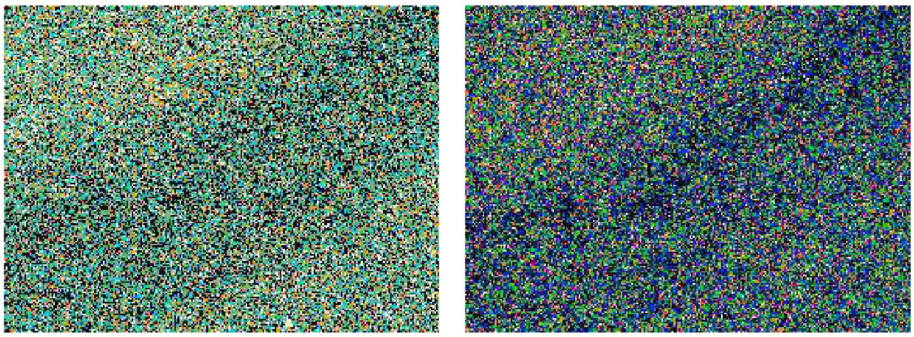

(d) C content (e) N content

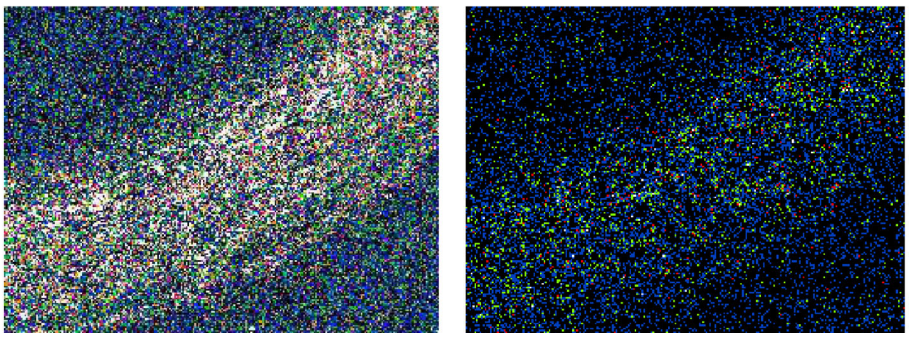

(f) O content (g) Si content

Fig. 6 Plane scans of worn scar on TiCN coating at 300 °C. **a** Scanned position. **b** Result of plane scan. **c** Ti content. **d** C content. **e** N content. **f** O content. **g** Si content

with those at 200 °C, and the plane scans of Ti, C, and Ti elements in Fig. 6c–e were darker, which indicated that the atom fractions on the worn scar were further decreased. But the content of O element increased from 14.35 to 20.37 %, which was expressed with the brighter zone of the O atom on the worn scar, as shown in Fig. 6f, showing that the TiCN coating occurred more serious oxidation wear and abrasive wear. The presence of Si atom was due to the transmission of the grinding ball to the coating surface, as shown in Fig. 6g.

3.5.3 Plane scan analysis of worn scar at 400 °C

Figure 7a shows the plane scanned position of worn scar at 400 °C, compared with those at 200 and 300 °C, the edge of worn scar appeared a few rough furrows. This was because the coating maintained the corresponding hardness at the temperature and was equivalent to the stabile polishing wear. Moreover, the grinding ball acted on the oxidized and softened coating, forming a relatively rough worn scar. The plane scan result of worn scar was shown in Fig. 7b; the mass fractions (mass, %) were Ti 45.86, C 14.37, N 15.99, O 23.43, and Si 0.35, and the atom fractions (at, %) were Ti 20.02, C 25.10, N 23.94, O 30.68, and Si 0.26. The worn scar had clear traces of spalling at the wear direction; the wear was heavily worn with the black belts at the edges of worn scar. In addition, the other zones were relatively uniform, which was due to spalling of the coating particles, resulting in a plough cutting effect, as shown in Fig. 7c–e. The plane scan of O element was brighter than those at 200 and 300 °C, showing that the TiCN coating was further oxidized with the temperatures increasing and

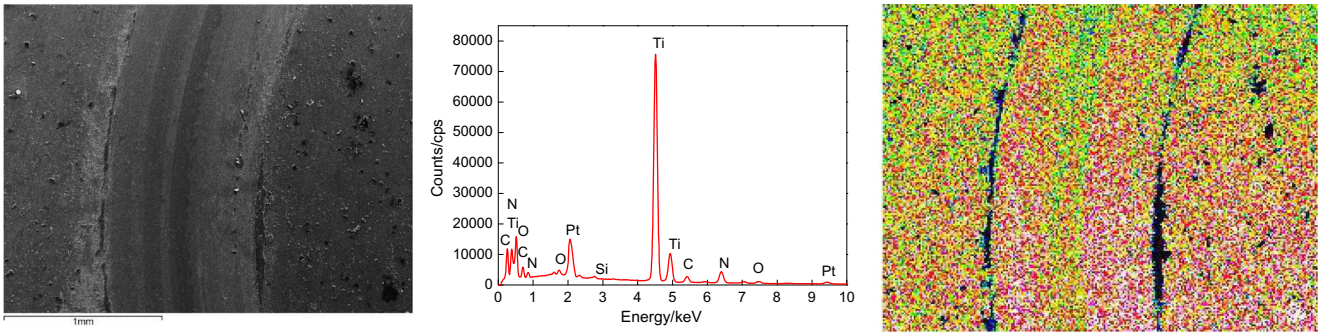

(a) Scanned position (b) Result of plane scan (c) Ti content

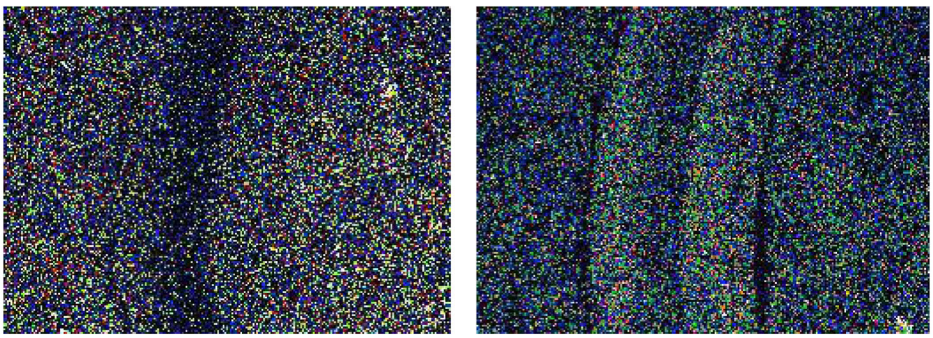

(d) C content (e) N content

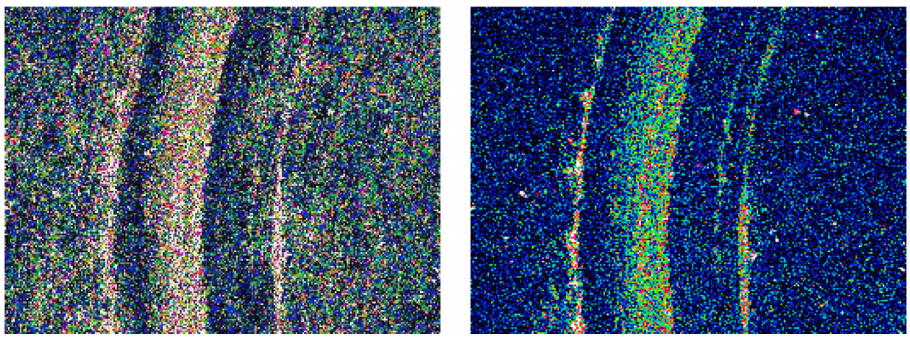

(f) O content (g) Si content

Fig. 7 Plane scans of worn scar on TiCN coating at 400 °C. **a** Scanned position. **b** Result of plane scan. **c** Ti content. **d** C content. **e** N content. **f** O content. **g** Si content

generated more TiO_2 films, acting as the effect of lubricant and antiabrasion, as shown in Fig. 7f. The plane scan of Si element was also brighter than that at 200 and 300 °C, which indicated that the wear of grinding ball was more serious with

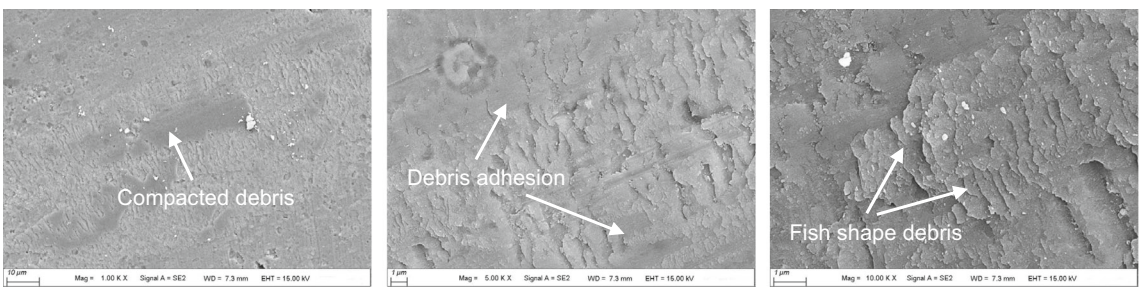

(a) Compacted debris (b) Debris adhesion (c) Fish shape debris

Fig. 8 Worn morphologies of the TiCN coating at 200 °C. **a** Compacted debris. **b** Debris adhesion. **c** Fish shape debris

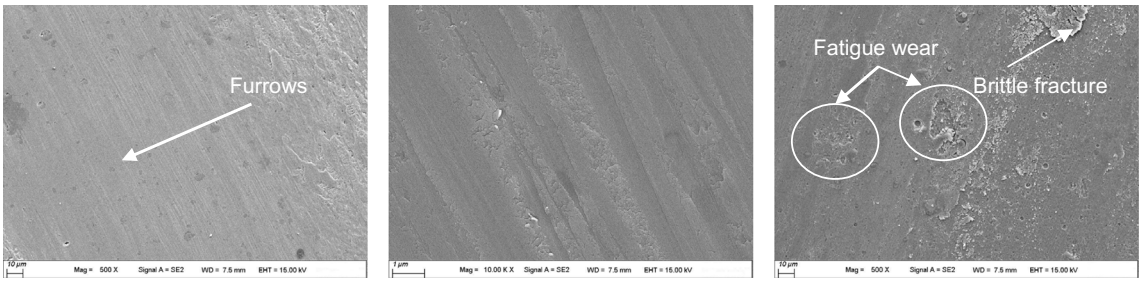

(a) Furrows (b) Abrasion wear (c) Fatigue wear

Fig. 9 Worn morphologies of TiCN coating at 300 °C. **a** Furrows. **b** Abrasion wear. **c** Fatigue wear

the temperature increasing and was transferred to the coating surface, as shown in Fig. 7g.

3.6 Mechanisms of friction and wear

Figure 8a shows the worn morphology of the TiCN coating at 200 °C; the worn scar surface was rougher, which was divided into the debris-compacted zone and debris adhesive zone. The formation of compacted debris zone was that the contact stress increased at the center of friction track, the worn debris was polished and compacted to accumulate in the center of worn scar, and the entire zone was rough. There were a lot of debris layers accumulating on the debris adhesion zone, appearing as the densely scaly debris at the rubbing direction, as shown in Fig. 8b. This was mainly because more debris were produced during the wear and the debris were not completely discharged friction track, forming a tongue-shaped adhesive with the moving of friction pair, showing an adhesive wear mechanism, as shown in Fig. 8c, which involved plastic grooving and chipping of the coating or coating detachment.

Figure 9a shows the morphology of the worn scar of the TiCN coating at 300 °C. Compared with that at 200 °C, the wear of the coating increased and the surface was rougher. There were a large number of worn debris layers that stayed and many fine furrows at the center of worn scar. There were smaller grinding grains acting as a role of macrocutting, shown in Fig. 9b; the furrow morphologies showed an obvious abrasion wear mechanism, which was responsible for the removal of material in the absence of coating detachment, depending on the hardness of the coating at a scale relevant to the contact stresses introduced by the asperities during the wear. A lot of white and bright colored oxide particles were produced during the wear; the oxidation products were mainly composed of TiO_2, which acted as the effect of lubrication and antifriction. The coating occurred as brittle fracture, and an amount of debris was formed by the fracture damages; under the bigger circulated friction stress, the large particles on the coating surface occurred as the fatigue fracture and gradually expanded, showing fatigue wear mechanism [18], as shown in Fig. 9c. The coating produced fatigue cracking and detachment, caused by the substrate hardness and toughness under localized contact stresses during the wear.

Figure 10a shows the worn morphology of TiCN coating at 400 °C. The coating wear was very serious; there was an amount of wear debris on the worn scar. The large debris adhered on the coating surface was a tongue, showing adhesive wear mechanism. The coating also occurred as the plastic deformation, as shown in Fig. 10b; this was because the hardness of the friction ball material (Si_3N_4) was about 16 GPa [19], resulting in the plastic deformation of the coating when the friction pairs on the softened TiCN coating. The coating oxidation at 400 °C was more serious and produced the TiO_2 with white bright color adhered on the worn scar. The oxidation wear was the oxidation of TiCN coating at temperatures over 300 °C [20], because TiO_2 species occurred on the coating surface, causing the coating strength to reduce, which showed obvious oxidation wear mechanism, as shown in Fig. 10c.

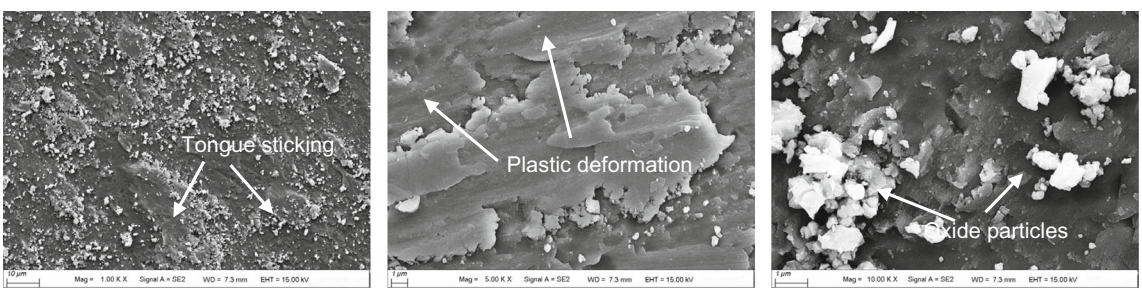

(a) Tongue sticking (b) Plastic deformation (c) Oxide particles

Fig. 10 Worn morphologies of the AlTiN coating at 400 °C. **a** Tongue sticking. **b** Plastic deformation. **c** Oxide particles

4 Conclusions

(1) The atoms of Ti, C, and N are closely bonded at the interface of the coating-substrate, forming a metallurgical bonding with the bonding strength of 58.15 N.
(2) The average COFs of TiCN coating at 200, 300, and 400 °C are 0.2931, 0.5252, and 0.4114, respectively, which increase firstly and then decrease with the temperature, and the wear rates gradually increase with the temperature, in which the TiO_2 plays the effect of lubrication and antifriction.
(3) The oxidation of TiCN coating is more serious with the temperature; the wear mechanisms of TiCN coating at high temperatures are primarily composed of oxidation wear, abrasive wear, and adhesive wear, accompanied by slight fatigue wear.

Acknowledgments Financial support for this research by the Jiangsu Province Science and Technology Support Program (Industry) (BE2014818) is gratefully acknowledged.

References

1. Aslantas K, Ucun İ, Çicek A (2012) Tool life and wear mechanism of coated and uncoated Al_2O_3/TiCN mixed ceramic tools in turning hardened alloy steel. Wear 274–275:442–451
2. Chinchanikar S, Choudhury SK (2015) Cutting force modeling considering tool wear effect during turning of hardened AISI 4340 alloy steel using multi-layer TiCN/Al_2O_3/TiN-coated carbide tools. Int J Adv Manuf Technol. doi:10.1007/s00170-015-7662-5
3. Kong DJ, Fu GZ (2015) Nanoindentation analysis of TiN, TiAlN and TiAlSiN coatings prepared by cathode ion plating. Sci China Technol Sci 58(1):1360–1368
4. Rasool G, Mridha S, Stack MM (2015) Mapping wear mechanisms of TiC/Ti composite coatings. Wear 328–329:498–508
5. Yang YL, Zhang D, Yan W, Zheng YR (2010) Microstructure and wear properties of TiCN/Ti coatings on titanium alloy by laser cladding. Opt Lasers Eng 48:119–124
6. Ren XY, Peng ZJ, Hu YB, Wang CB, Fu ZQ, Yue W, Qi LH, Miao HZ (2013) Abrasive wear behavior of TiCN cermets under water-based slurries with different abrasives. Tribol Int 66:35–43
7. Bonny K, De Baets P, Vleugels J et al (2008) Reciprocative sliding wear of ZrO_2-TiCN composites against WC-Co cemented carbide. Wear 265(11–12):1767–1775
8. Vereschaka A, Volosova MA, Batako AD, Vereshchaka AS, Mokritskii BY (2015) Development of wear-resistant coatings compounds for high-speed steel tool using a combined cathodic vacuum arc deposition. Int J Adv Manuf Technol. doi:10.1007/s00170-015-7808-5
9. Liu Y, Huang CZ, Liu HL, Zou B (2015) Mechanical properties and microstructure of Ti(C_5N_5)-TiB_2-(W_7Ti_3)C composite cutting tool materials. Int J Adv Manuf Technol 79:949–957
10. Zou B, Chen M, Li SS (2011) Study on finish-turning of NiCr20TiAl nickel-based alloy using Al_2O_3/TiN-coated carbide tools. Int J Adv Manuf Technol 53:81–92
11. Kong DJ, Guo HY (2015) Friction-wear behaviors of AlTiN coating by cathodic arc ion plating at high temperatures. Tribol Int 88:31–39
12. Downey J, O'Leary P, Raghavendra R (2014) Comparison and analysis of audible sound energy emissions during s ingle point machining of HSTS with PVD TiCN cutter insert across full tool life. Wear 313(1–2):53–62
13. Tang AT, Chen M, Wang J, Liu CP, Pan FS, Wang WQ (2011) Phase evolution during carbothermic reduction process of ilmenite for TiCxN1-x composite powders. Rare Metal Mater Eng 40(S3):281–285
14. Li JL, Zhang SH, Li MX (2013) Influence of the C_2H_2 flow rate on gradient TiCN films deposited by multi-arc ion plating. Appl Sur Sci 283:134–144
15. Aramcharoen A, Mativenga PT (2008) White layer formation and hardening effects in hard turning of H13 tool steel with CrTiAlN and CrTiAlN/MoST-coated carbide tools. Int J Adv Manuf Technol 36:650–657
16. Feng WR, Zhou H, YangS Z (2010) Nano-indentation and wear-resistance behaviors of TiCN films by pulsed plasma on cemented carbide cutting tool. Mater Sci Eng A 527:4767–4770
17. Meng JH, Lu JJ, Wang JB, Yang SR (2006) Tribological behavior of TiCN-based cermets at elevated temperatures. Mater Sci Eng A 418:68–76
18. Wang QZ, Zhou F, Chen KM, Wang ML, Qian T (2011) Friction and wear properties of TiCN coatings sliding against SiC and steel balls in air and water. Thin Solid Films 519:4830–4841
19. Wang QZ, Zhou F, Gao S, Zhou ZF, Li LKY, Yan JW (2015) Effect of counterparts on the tribological properties of TiCN coatings with low carbon concentration in water lubrication. Wear 328–329:356–362
20. Polcar T, Kubart T, Novák R, Kopecký L, Široky Ṕ (2005) Comparison of tribological behaviour of TiN, TiCN and CrN at elevated temperatures. Surf Coat Technol 193:192–199